Application of Proper Orthogonal Decomposition to the morphological analysis of confined co-axial jets of immiscible liquids with comparable densities

Georgios Charalampous and Yannis Hardalupas

Citation: Physics of Fluids (1994-present) **26**, 113301 (2014); doi: 10.1063/1.4900944
View online: http://dx.doi.org/10.1063/1.4900944
View Table of Contents: http://scitation.aip.org/content/aip/journal/pof2/26/11?ver=pdfcov
Published by the AIP Publishing

PHYSICS OF FLUIDS **26**, 113301 (2014)

Application of Proper Orthogonal Decomposition to the morphological analysis of confined co-axial jets of immiscible liquids with comparable densities

Georgios Charalampous[a] and Yannis Hardalupas
Department of Mechanical Engineering, Imperial College London, London SW7 2AZ, United Kingdom

(Received 4 February 2014; accepted 14 October 2014; published online 5 November 2014)

The development of a round liquid jet under the influence of a confined coaxial flow of an immiscible liquid of comparable density (central to annular flow density ratio of 8:10) was investigated in the vicinity of the nozzle exit. Two flow regimes were considered; one where the annular flow is faster than the central jet, so the central liquid jet is accelerated and one where the annular flow is slower, so the central liquid jet is decelerated. The central jet was visualised by high speed photography. Three modes of jet development were identified and classified in terms of the Reynolds number, Re, of the central jet which was in the range of $525 < \mathrm{Re} < 2725$, a modified definition of the Weber number, We, which allows the distinction between accelerating and deceleration flows and was in the range of $-22 < \mathrm{We} < 67$ and the annular to central Momentum Ratio, MR, of the two streams which was in the range of $3.6 < \mathrm{MR} < 91$. By processing the time resolved jet images using Proper Orthogonal Decomposition (POD), it was possible to reduce the description of jet morphology to a small number of spatial modes, which isolated the most significant morphologies of the jet development. In this way, the temporal and spatial characteristics of the instabilities on the interface were clearly identified which highlights the advantages of POD over direct observation of the images. Relationships between the flow parameters and the interfacial waves were established. The wavelength of the interfacial instability was found to depend on the velocity of the fastest moving stream, which is contrary to findings for fluids with large density differences. [http://dx.doi.org/10.1063/1.4900944]

I. INTRODUCTION

The development of a round liquid jet in an environment of an immiscible fluid has been the focus of many investigations as reviewed in Refs. 1–3. The initial development of the interfacial boundary between the two phases determines the growth of the instabilities on the jet surface, which subsequently controls the dispersion of the two phases downstream. Therefore, the investigation of the initial stages of jet development is important for the understanding of the development of the flow downstream and the breakup process of the central jet core. A considerable amount of research has been performed on the development of liquid jets in gas environments, which can generally be classified in two categories.[4–8] In the first, the jet is injected into a quiescent environment as is the case of pressure atomisers. In the latter, a relatively slow moving central liquid jet is atomised by a high speed coaxial gas stream as is the case of air-blast atomisation. While superficially the difference between the two processes might appear to be only in the frame of reference, practically the two processes are substantially different. In the former the central jet is compacted, while in the

[a]Author to whom correspondence should be addressed. Electronic mail: georgios.charalampous@imperial.ac.uk

latter the central jet becomes elongated due to momentum transfer between the two streams leading to deceleration and acceleration of the central jet, respectively. This behaviour was discussed and its importance demonstrated by Domann and Hardalupas.[9] It is thus necessary to consider the cases of accelerated and decelerated jets separately, as was initiated by Charalampous *et al.*[10] For liquid in liquid jet flows, while there has been experimental work on the development of a liquid jet in a quiescent liquid environment,[11–16] experimental work on the destabilization of round liquid jets by a coaxial liquid stream is generally limited to microfluidics applications.[17–19] However, the mixing of coaxial jets is also important for other applications. For example, in mixers the destabilization of the central jet will determine the degree of mixing of the two phases. In chemical reactors, the speed of the chemical reaction is determined by the interfacial area, which, in turn, depends on the dispersion of the two phases. The extrapolation of the findings of similar types of flow might not be adequate for the description of these processes. For example, due to the vastly different density ratios between liquid and gas or of the extremely small Reynolds numbers in the microfluidic flows, the conclusions of these investigations will be unlikely to apply to liquid-liquid interactions with large Re. It is the purpose of this paper to investigate the morphology of a liquid jet in the vicinity of the jet nozzle exit, as it develops under the influence of a coaxial stream of an immiscible liquid. By confining the two streams within a tubular chamber, the flows of the two phases can be accurately controlled. Flow conditions, where the central jet is accelerated or decelerated due to transfer of momentum from or to the annular flow, respectively, can be obtained and a range of flow regimes can be identified. The focus of the investigation is on the transition from accelerated to decelerated central jets, since it is in this region that the most radical changes in the jet morphology are expected to occur.

For the analysis of the morphology of the central jet beyond the direct observation of the jet characteristics, the Proper Orthogonal Decomposition (POD) method will be used. This method was originally proposed by Pearson[20] for the optimal description of multidimensional datasets when reducing the number of dimensions. In the context of fluid mechanics, the use of the POD method was proposed by Lumley for the analysis of the velocity field[21] and has been used extensively since then for the analysis of the flowfield.[22] In the context of image description, which is of interest here, POD was initially proposed for the identification of human facial features[23] and later the technique was applied to the investigation of the morphology of the structure of a liquid jet in a gas cross-flow.[24] There, the analysis of time resolved photographic images of the liquid jet, revealed a large number of independent overlapping modes of spatial development that contributed to the overall jet morphology. Travelling waves were found to exist on the liquid jet surface, which would not be detected directly, some of which matched the wavelength predicted by the Kelvin-Helmholtz instability. Due to the intense atomisation conditions considered in that investigation, a large number of modes had to be superimposed for an adequate description of the liquid jet. For the jets of the current investigation, we consider less intense interaction between the two streams for either for accelerated or decelerated central liquid jets and jet morphologies that are not chaotic can be expected, so that a more definite description of their characteristics can be derived.

The paper is structured as follows. First the experimental arrangement is described, along with the instrumentation and the range of considered flow conditions. In Sec. III, the morphology of the central jet is classified based on the initial flow conditions. A breakdown of the overall morphology of the liquid jet is presented in Sec. IV, where POD is used to analyse the spatial and temporal characteristics of the most energetic features of the liquid jet. Next the findings of Secs. III and IV are discussed and the advantages of the POD method are highlighted. The paper closes with a summary of the conclusions.

II. EXPERIMENTAL ARRANGEMENT

This investigation was conducted within a channel formed by a transparent acrylic chamber. Within the channel a circular oil jet was injected centrally and developed under the influence of a coaxial water stream. The diameter of central oil jet was $D_1 = 3.3$ mm. The cross section of the chamber is shown schematically in Figure 1. The channel was segmented in three stages. The first stage was a contraction that accelerated the annular water flow. The central jet nozzle was contained

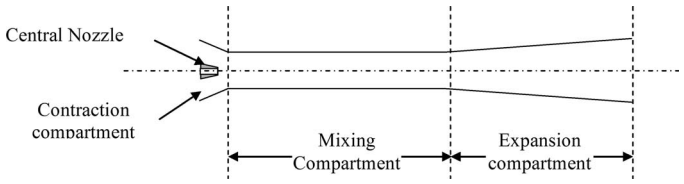

FIG. 1. Geometry of the test chamber comprising of three compartments and the central jet nozzle.

here. The next stage was a circular cylinder with a diameter $D_2 = 12$ mm ($3.6D_1$) that extended for about $21D_1$. Here the central oil jet developed under the influence of the coaxial water stream. The final stage was a conical expansion. Its purpose was to decelerate the mixed oil/water flow before the test chamber exit. The central jet nozzle was straight and had a length of $35D_1$. The internal nozzle diameter was about $2.3D_1$ which means that the oil flow developed inside the nozzle for about 15 diameters. The tip of the central nozzle was a conical contraction with an area ratio of about 5. Therefore, the mean velocity profile of the jet was fairly uniform with relatively thin boundary layer. The oil flow was supplied at the base of the nozzle by three separate inlets, which ensured an axisymmetric flow. The nozzle was aligned coaxially to the central axis of the annular flow and its exit was placed one nozzle internal diameter upstream of the entry of the mixing compartment.

The two working liquids were kerosene-based oil Clairsol 350 for the central jet and water from the main supply for the annular flow. The density, ρ, and the dynamic viscosity, μ, of each liquid and the interfacial tension, σ, between the two liquids are summarised in Table I. Due to the high interfacial tension between the two fluids and, therefore, insignificant miscibility, the sharp interface formed between the two resulted in a clear optical depiction of the interfacial boundary.

Figure 2 shows a schematic of the control circuit of the two liquids. The water and oil parts of the flow circuit are indicated in dark gray and light gray, respectively. About 500 l of each of the pure liquids were stored in tanks (A) for water and (B) for oil. Water and oil were pumped in the test chamber (J) by pumps (E) and (G), respectively. Both pumps operated at constant speeds. The flowrate of the pumped liquids was adjusted by valves (D) for water and (F) for oil. The valves either limited the flow to the test chamber or returned excess flow back to the storage tanks. The flow rate of water that was delivered to the test chamber was monitored by rotameter (H) and the flow rate of oil that was delivered to the test chamber was monitored by rotameter (I). The annular water flow was conditioned before entering the test chamber through contraction (L), which had a 9:1 area ratio to ensure the uniformity of the velocity profile of the annular water flow. The transparent test chamber was positioned vertically and exhausted upwards in a vertical column (K) that was 2 m long. The vertical mounting of the test chamber has a number of advantages. The first is that the central jet, which conveys the lighter liquid, is gravitationally stable. In this way, there is no possibility of backflow, which would be possible if the central jet was heavier than the annular liquid. Also, the features along the oil-water interface can develop axi-symmetrically. This might not be the case, if the jet was injected in the horizontal direction, due to gravity. Another benefit of the vertical configuration is that the height of liquid in the system is kept constant by a drain at the top of the vertical column. Since the volume of column (K) is filled with water at the beginning of the experiment and the oil from the jet is buoyant and rises to the top where it is drained, the oil concentration in the column does not exceed 3% during the operation of the system. Therefore, the pressure at the exit of the test chamber is always constant at about 2 m of H_2O. The mixed flow at the

TABLE I. Physical properties of the two liquids.

	ρ (Kg/m^3)	μ (Pa s)	σ (N/m)
Water	1000	0.0010	0.048
Clairsol 350	805	0.0019	

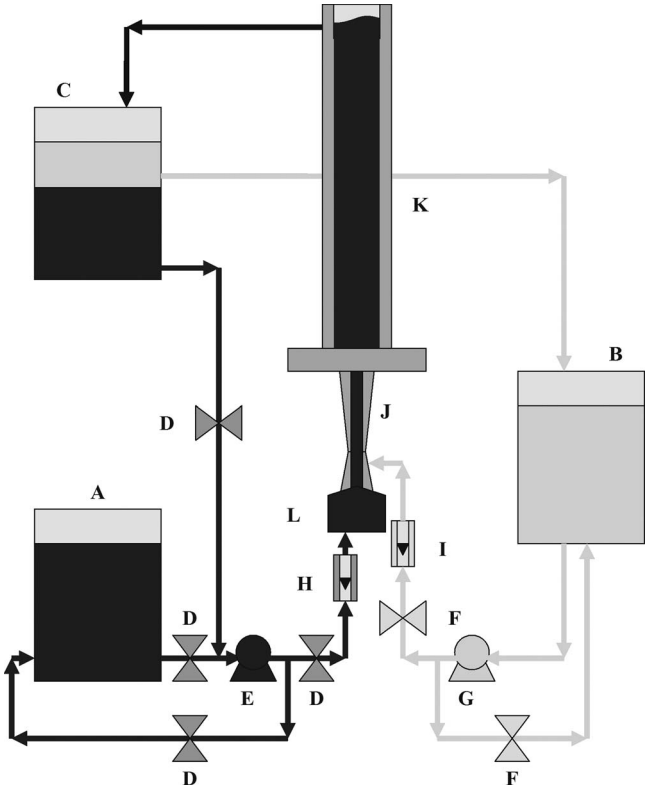

FIG. 2. Schematic of the experimental arrangement of flow circuit of the coaxial jets, which are injected in the transparent test chamber (J). Water circuit is shown in dark gray and oil circuit is shown in light gray.

exit of the vertical column (K) was drained to tank (C), where the two phases were left to separate so that they could be reused.

The flow in the test chamber was visualised by high speed photography. The light source was a 100 W lamp, which back-illuminated the test chamber. Imaging of the flow was conducted with a Photron APX 10-bit CMOS placed in front of the test chamber. The camera was fitted with a 105 mm macro lens, which allowed a close distance between the camera and the flow that resulted to a spatial resolution of the acquired images of about 45 μm/pixel. Due to the large size of the acquired images in the full frame resolution of 1024 $\times$ 1024 pixels, the utilised region of the camera sensor was reduced to 320 $\times$ 1024 pixels. This was adequate to image the full width of the vertically oblong channel and the reduction of the dataset size was considerable. The imaging rate was set to 10 000 fps. This is sufficient to temporally resolve phenomena up to 5000 Hz, which is more than adequate for the frequencies of the investigated flows, which were in the region of 250 Hz.

Both accelerating and decelerating central jets were considered. The characteristic velocities U_1 of the central jet stream and U_2 of the coaxial flow were calculated from their volumetric flowrates, as area averaged velocities of the cross section at the nozzle exit. The velocity U_1 of the central jet was in the range of 0.39 m/s and 1.95 m/s and U_2 of the annular flow was set to 0.96 m/s.

In addition to the velocities of the two streams, the central jet liquid density ρ_1 and dynamic viscosity μ_1, the annular jet liquid density ρ_2 and dynamic viscosity μ_2, the interfacial tension σ, and the characteristic lengths of the central and annular jets D_1, $\sqrt{D_2^2 - D_1^2}$ can be expected to influence the flow. Therefore, there are nine dimensional quantities in total that can affect the flow. Considering that there are three dimensions to the problem, namely time, length and mass, the description of the flow can be reduced to 6 independent dimensionless parameters. The six dimensionless parameters are estimated by considering the product of three basic dimensional quantities and one of the remaining dimensional quantities. The three basic dimensional quantities are raised to appropriate

powers, so that the derived quantity is dimensionless:

$$D_1^a \cdot \rho_1^b \cdot U_1^c \cdot \mu_1, \tag{1}$$

$$D_1^a \cdot \rho_1^b \cdot U_1^c \cdot \sigma, \tag{2}$$

$$D_1^a \cdot \rho_1^b \cdot U_1^c \cdot U_2, \tag{3}$$

$$D_1^a \cdot \rho_1^b \cdot U_1^c \cdot \rho_2, \tag{4}$$

$$D_1^a \cdot \rho_1^b \cdot U_1^c \cdot \mu_2, \tag{5}$$

$$D_1^a \cdot \rho_1^b \cdot U_1^c \cdot \sqrt{D_2^2 - D_1^2}. \tag{6}$$

With appropriate arrangement of the terms and following the rules of dimensional analysis,[25] the relevant dimensionless parameters are as follows.

The Reynolds number (Re) of the central jet, estimated as

$$\mathrm{Re} = \frac{\rho_1 \cdot U_1 \cdot D_1}{\mu_1}, \tag{7}$$

describes the relative importance between the inertial and the central forces on the central jet. For the velocities of interest, the range of Re spanned between 545 and 2725, which covers laminar to transitional jets.

The Weber number as defined by Weber[26] and the dimensional analysis is

$$We = \frac{\rho_2 \cdot U_1^2 \cdot D_1}{\sigma}, \tag{8}$$

where ρ_2 is the annular stream density and σ is the interfacial tension between the two liquids. In order to take into account the relative velocity of the two streams the Weber is usually modified to

$$We = \frac{\rho_2 \cdot (U_1 - U_2)^2 \cdot D_1}{\sigma}, \tag{9}$$

which is the most widely used expression and is indicative of the ratio between the inertial and the surface tension forces acting on the central jet. We introduce a further variation of We from Eq. (9):

$$We = \frac{\rho_2 \cdot |U_1 - U_2| \cdot (U_1 - U_2) \cdot D_1}{\sigma}. \tag{10}$$

The absolute magnitude of We between Eq. (9) and the current definition of Eq. (10) are exactly matched, but, in the latter, the sign is positive when the central jet is decelerated and negative when the central jet is accelerated. This definition attempts to account for the effect of direction of the acceleration of the central jet, which can influence the evolution of the flow. As the physical properties of the two flow components were not changed in this investigation, We effectively capture the effect of the shear between the two streams. For the range of flow conditions the value of We is $-22 < \mathrm{We} < 67$, which covers cases with limited influence of hydrodynamic effects between the two streams ($\mathrm{We} \sim 0$) and cases where the hydrodynamic effects are significant ($|\mathrm{We}| > 10$) and the momentum ratio (MR) of the two. For completeness, both numbers were considered.

While the We number describes the potential for hydrodynamic effects to develop, it does not offer insight on the potential of these effects to grow along the interface. This can be described by the ratio of the momentum of the annular stream to the momentum of the central stream:

$$MR = \frac{\rho_2 \cdot U_2^2 \cdot A_2}{\rho_1 \cdot U_1^2 \cdot A_1}, \tag{11}$$

where A_1 is the cross sectional area of the central nozzle and A_2 the cross sectional area of the annulus $A_2/A_1 = \left(D_2^2 - D_1^2\right)/D_1^2$.This definition allows the consideration of MR in the case where

TABLE II. Flow conditions and uncertainties.

U_1 (m/s)	U_2 (m/s)	Re	We	MR
0.39 ± 0.10	0.96 ± 0.16	545 ± 136	-22.1 ± 20.0	91.4 ± 38.1
0.78 ± 0.10	0.96 ± 0.16	1090 ± 136	-2.2 ± 6.3	22.8 ± 6.6
1.17 ± 0.10	0.96 ± 0.16	1635 ± 136	3.1 ± 7.5	10.1 ± 2.5
1.36 ± 0.10	0.96 ± 0.16	1907 ± 136	11.4 ± 14.4	7.4 ± 1.7
1.57 ± 0.10	0.96 ± 0.16	2180 ± 136	24.9 ± 21.3	5.7 ± 1.3
1.95 ± 0.10	0.96 ± 0.16	2725 ± 136	67.7 ± 35.0	3.6 ± 0.7

the annular stream is stationary and the central jet develops in a confined quiescent environment. The MR varies from 3.6 to 91. For large values of MR, the momentum of the annular flow is greater than the momentum of the flow of the central jet. Therefore, it is expected for the annular flow to dominate the development of the central jet, so that there is a one way coupling between the two streams. For values approaching unity, the momentum of both streams is of the same order, so it is expected that there will be a two way coupling between the two streams.

The three above quantities include the velocities of the streams in their definitions and have been extensively used to characterise the stability of liquid jets are[3,27] in terms of dynamic influences.

Out of the three remaining dimensionless quantities, two describe purely physical influences and one is purely geometric. There quantities are

the density ratio,

$$\frac{\rho_2}{\rho_1}, \tag{12}$$

the viscosity ratio,

$$\frac{\mu_2}{\mu_1}, \tag{13}$$

and the characteristic length ratio,

$$\frac{\sqrt{D_2 - D_1}}{D_1}. \tag{14}$$

As in this investigation, the liquids of the two streams and the flow chamber geometry remained the same, the values of the three above quantities are fixed to 0.8, 0.52, and 3.5, respectively.

The values of the dynamic parameters that describe the flow are tabulated in Table II along with the uncertainties due to the limited resolution of the rotameters that measured the flow rates of each stream.

III. MORPHOLOGY OF THE CENTRAL LIQUID JET

The morphology of the central jet is described in terms of the dominant features that develop on the oil-water interface, as determined by photography. Overall three modes of development of the central jet were observed. Examples of the observed modes are presented in Figure 3 and include straight jet, varicose jet, and "cup" shaped jet. The differences between the central jet development modes depend on the Re, We, and MR of the flow as discussed in the following text.

A. Straight jet

This type of flow appears when We is negative or near zero. The central jet develops as a straight liquid column without remarkable surface features along its length. The lack of development demonstrates that the central jet is stable within the bounds of the imaged region. The diameter of the central jet depends on the magnitude of the We number as explained below.

Since the mean velocity of the annular flow is greater than the mean velocity of the central jet, the central jet is accelerated and the diameter of the central jet becomes smaller than the central

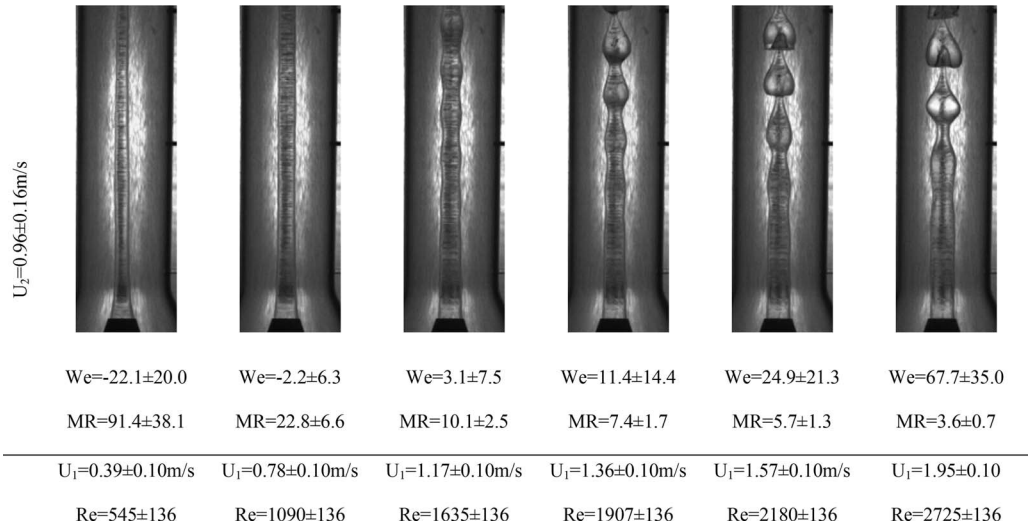

FIG. 3. Morphology of the developing central jet in the confined coaxial stream. The nozzle exit internal diameter is $D_1 = 3.3$ mm.

nozzle diameter, as expected from the conservation of mass. The final jet diameter is obtained very close to the nozzle exit, which shows that the two streams have attained the same velocity within a short distance from the nozzle exit and, therefore, the acceleration of the central jet is fast. The average spatial acceleration of the central jet was estimated as $\alpha \sim 88\ s^{-1}$ and $\alpha \sim 43\ s^{-1}$ for flows with $U_1 = 0.39$ m/s and $U_1 = 0.78$ m/s, respectively. The cause of the fast acceleration is that for this type of geometry the momentum ratio MR of Eq. (11) is very high with MR = 91.4 for $U_1 = 0.39$ m/s and MR = 22.8 for $U_1 = 0.78$ m/s. Therefore, the annular flow can accelerate the central stream, while the reverse effect is minor.

Since the two streams obtain similar velocities quickly downstream of the nozzle exit, it might be expected that the stability of the co-flow downstream will be controlled by the Rayleigh-Plateau mechanism, which manifests as regularly spaced dilatations along the length of the central jet. However, no such features were observed in the imaged area. The residence time of the annular stream in the imaged length is of the order of 50 ms and, since the central jet is quickly accelerated to the speed of the annular stream, this is also the residence time of the central jet in the imaged region. It is likely that the residence time of the jet along the length of the channel is not sufficient for this type of instability to develop. Therefore, the straight jet flow regime is stable within the test chamber.

B. Varicose jet

When the We number becomes slightly positive ($0 < We < 12$), the central jet is decelerated by the annular stream and its morphology changes drastically in comparison to $We < 0$. The previously featureless central core now develops convex axi-symmetric dilatations along its length. The distance between successive dilatations is constant along the length of the jet, while the amplitude of the dilatations increases downstream of the nozzle. Nevertheless, the dilatations retain their overall convex shape throughout the imaged region.

As the dilatations appear immediately after the transition from a negative to a positive We, it is likely that the cause of the dilatations is of hydrodynamic origin due to the deceleration of the jet. It can then be argued that the deceleration of the central jet by the coaxial flow of another liquid generates stronger instability on the jet surface than the acceleration of the jet. After the instability is initiated by hydrodynamic effects, its growth is likely mediated by interfacial tension, since the shear between the two streams is generally low considering the We number of the flows.

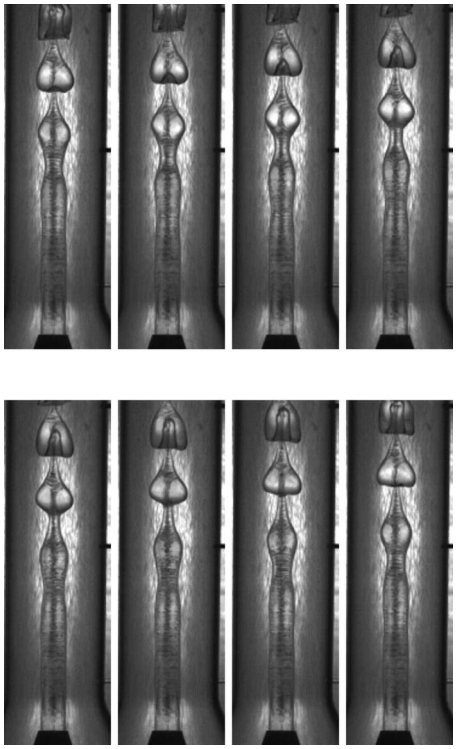

FIG. 4. Time series of cup formation for a flow with Re = 2725, We = 67.7, and MR = 3.6. The time step between successive snapshots of the flow is 0.6 ms. The nozzle exit internal diameter is $D_1 = 3.3$ mm.

Due to the vertical geometrical arrangement of the experiment, gravitational effects would favour stability of the accelerated jet as both gravity would promote the stretching of the central jet. However, the time scales involved (it was found that a droplet in a quiescent chamber requires several hundreds of ms to travel through the imaged region) are significantly greater than the residence time in the imaged region (several tens of ms), which makes this case unlikely.

C. "Cup" shaped jet

Increasing the value of the We number over 25 causes the varicose instabilities to develop further. Unlike the case of the varicose dilatations, which developed in amplitude but maintained the same shape along the jet length, for this type of flow the amplitude of the dilatations increases and simultaneously the shape of the dilatations deforms with distance from the nozzle. This is the result of the stronger hydrodynamic shear for the higher We number regime. Additionally, the annular to central jet momentum ratio of Eq. (11) is lower than before, which means that progressively the one way influence of the central jet by the annular flow of the varicose flow regime changes to a two way interaction, where both streams affect each other and there is entrainment from the central jet to the annular stream.

Because this flow regime is more dynamic, it will be described through a series of temporally correlated images, which are presented in Figure 4. The instability begins as an axi–symmetric convex dilatation. As in the case of the varicose type jets, the amplitude of the dilatation grows along the jet length. However, in this case, due to the deceleration of the central jet surface, the rim of the dilatation is sheared and the initial convex dilatation deforms and follows a piriform. The rim is further stretched in the direction of the nozzle to form a curtain, which envelopes the central jet core. This process is repeatable and sequential structures are formed, which are reminiscent of stacked cups.

The configuration of a long thin lamella is inherently unstable and it is expected to collapse downstream, either under the influence of interfacial tension or due to collision between successive "cup" structures that have grown sufficiently to cover the distance between them.

IV. APPLICATION OF PROPER ORTHOGONAL DECOMPOSITION TO THE EVALUATION OF THE LIQUID JET MORPHOLOGY

In the previous section the morphology of the central jet was qualitatively described in the context of the features that develop along the central jet surface. Here a more detailed description is provided by breaking down the morphology of the developing oil jet to independent spatial POD modes. In order to determine the basic structures of the jet morphology, coherent spatial POD modes that capture significant proportion of the image intensity fluctuations are sought. While it may seem reasonable that the analysis of the acquired images with POD will identify these structures, it is not necessarily so, as it has been demonstrated that the salient morphological features might be rather obscured among less interesting structures.[24] Nevertheless, due to the relatively simple geometry of the flow in this investigation, useful results were obtained.

The POD method for application to fluid flow photographic images has been described in detail before.[24] Therefore, we provide only a summary of the methodology here. From the image acquisition, a dataset of N image samples with a resolution of X × Y pixels is obtained. Each image $\mathbf{x_i}$ is considered a vector in an X × Y dimensional space. This means that each pixel represents an individual dimension with its intensity as the vector magnitude. In the case of an image, all vectors have positive magnitudes. For the purposes of processing, the two-dimensional image matrix is rearranged in the linear shape of a vector. The mean image intensity of the sample is then computed for each pixel (dimension) and the resulting mean image intensity $\langle \mathbf{x_i} \rangle$ is subtracted from each sample $\mathbf{x_i}$, resulting to a dataset of N samples $\mathbf{y_i} = \mathbf{x_i} - \langle \mathbf{x_i} \rangle$, which contain the deviation of the intensity from the mean image intensity. Next the covariance between each of the dimensions is calculated resulting to an X × Y by X × Y matrix $\mathbf{C}$. The X × Y eigenvectors $\mathbf{f_i}$ of the covariance matrix $\mathbf{C}$ are the POD modes of the image dataset and express the optimal linear fit of an orthogonal basis to the acquired images $\mathbf{x_i}$. The corresponding eigenvalues $\mathbf{l_i}$ determine the amount of the contribution of each POD mode to the overall intensity fluctuations of the original images, with modes of larger $\mathbf{l_i}$ being more significant. For this reason the POD modes are arranged in order of descending $\mathbf{l_i}$. If the number of images N is less than the number of dimensions X x Y, only N POD modes will be identified since there is not sufficient information to fully resolve all orthogonal dimensions. In this case, the snapshots method can be used for the evaluation of $\mathbf{f_i}$ and $\mathbf{l_i}$ to save computational resources, since the size of the covariance matrix is reduced to N by N.

Information of the contribution of each POD mode to each image is obtained by projecting each image $\mathbf{y_i}$ on the POD mode $\mathbf{f_i}$, $a_i = \mathbf{y_i f_i}$. In this way, a series of N temporal coefficients are obtained for each mode, which describes the temporal dependency of the image sample on the POD modes. The power spectral density of the series of temporal coefficients can be used to resolve the temporal frequencies that dominate each POD mode, while the cross spectral density of the temporal coefficients of two POD modes can identify the correlation between the temporal frequencies of the POD modes and their phase relationships.

A. Varicose jet

First the varicose type instability of the central liquid jet flow is analysed. Although it can be claimed that due to the simplicity of this geometry it is not necessary to use POD for the breakdown of this morphology to its basic components, it will be shown that there are aspects of the jet morphology, which are better evaluated by POD than direct observation of the jet images.

For this type of flow, the first four POD modes contain sufficient information to describe the jet shape with enough accuracy to capture the main varicose structures, while higher order modes contain information which is not essential to the structure of the jet. The first two modes describe the basic dilatation that develops on the jet interface. The breakdown of the jet image into these modes is presented in Figure 5. The original image is shown in Figure 5(a), and the two first POD modes

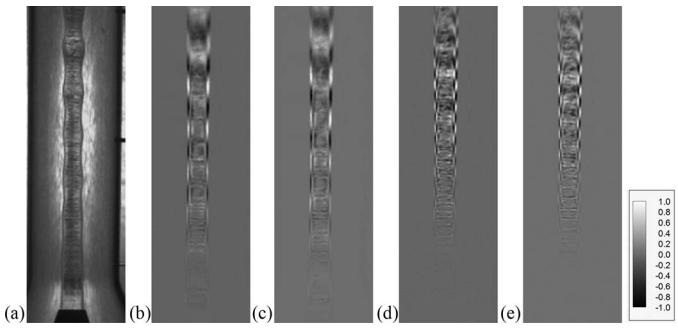

FIG. 5. Image sample of central jet (a) for flow Re = 1635, We = 3.1, and MR = 10.1, and the first four POD modes. Mode 1 (b) and 2 (c) represent the varicose dilatation, which propagates along the jet length. Mode 3 (d) and 4 (e) represent the second spatiotemporal harmonic of the varicose dilatation. The jet exit diameter is $D_1 = 3.3$ mm.

in Figures 5(b) and 5(c). The intensity deviations from the mean image appear in the POD modes as sequential white and black bands on the region of the jet surface. White indicates a positive deviation of the image intensity from the mean image, black a negative deviation and gray is indicative of no image intensity fluctuations. The scale of each POD mode is normalised in the range between −1 and 1 by the maximum absolute value of each POD mode, so that the coherence of the spatial characteristics that are captured by each mode can be displayed clearly. It can be observed that the white and black bands of the two first POD modes are complementary and overlap with each other if shifted by half a band length. Also, the length of two successive bands is equal to the wavelength of the varicose dilatation. The clarity of the boundary between successive bands makes it easy to determine the wavelength of the varicose waves, which is not easy if the distances between successive crests or troughs are used as these points are not well defined. The superimposition of the two first POD modes can reproduce the varicose dilatations with crests at any length along the jet length. The adequacy of the first two modes to reproduce the varicose jet is presented in Figure 6 for the flow with Re = 1635, We = 3.1, and MR = 10.1. The original jet image is shown in Figure 6(a), while Figure 6(b) shows the reconstructed jet using the two first POD modes. Despite some limited blurring of the fine details along the interface, the reconstruction is excellent. The reason is that the first two modes capture a significant amount of the image intensity fluctuations. For the presented example, each of the first two modes captures over 30% of the total image intensity fluctuations, as can be seen in Figure 7. Therefore, with a combined total of over 60% of the image intensity fluctuations, most of the image motion details are captured.

Only about 5% of the image intensity fluctuations are captured by each of modes 3 and 4 shown in Figures 5(d) and 5(e), respectively. However, if these two modes are also considered, further

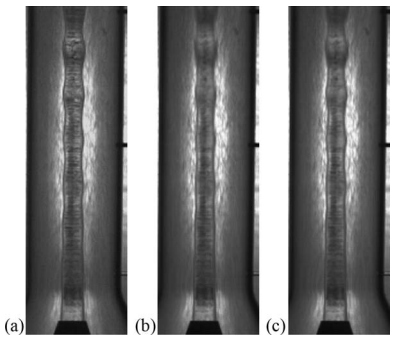

FIG. 6. Reconstruction of an image sample of flow Re = 1635, We = 3.1, and MR = 10.1. (a) Original image, (b) reconstruction of original image using modes 1 and 2, and (c) reconstruction of original image using modes 1–4. Modes 1 and 2 describe the basic varicose dilatation, which propagates along the jet length, and modes 3 and 4 represent the first spatiotemporal harmonic of the varicose dilatation. The jet exit diameter is $D_1 = 3.3$ mm.

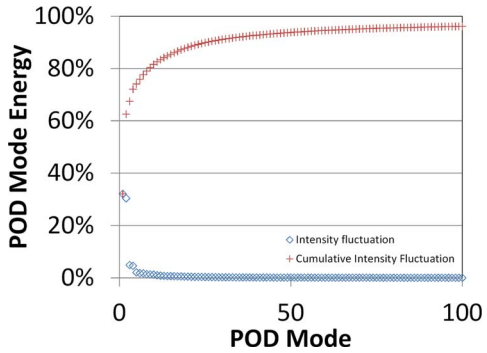

FIG. 7. Distribution of the normalised image intensity fluctuations that is captured by each POD mode and the cumulative normalised energy fluctuations. The first four modes capture over 70% of the overall image intensity fluctuations for flow Re = 1635, We = 3.1, and MR = 10.1.

improvement of the jet reconstruction quality is achieved (Figure 6(c)). The spatial distribution of the positive and negative bands of these modes is similar to modes 1 and 2, but the spatial scale of the bands in the horizontal and vertical direction is only half of modes 1 and 2. They represent the second harmonic of the varicose structures that develop on the jet surface. The consideration of more modes is not required since each further mode contains progressively less useful information.

The temporal analysis of the POD modes provides information on the periodicity of the features that are captured by each POD mode. In Figures 8(a) and 8(b), the Fourier transform of the temporal

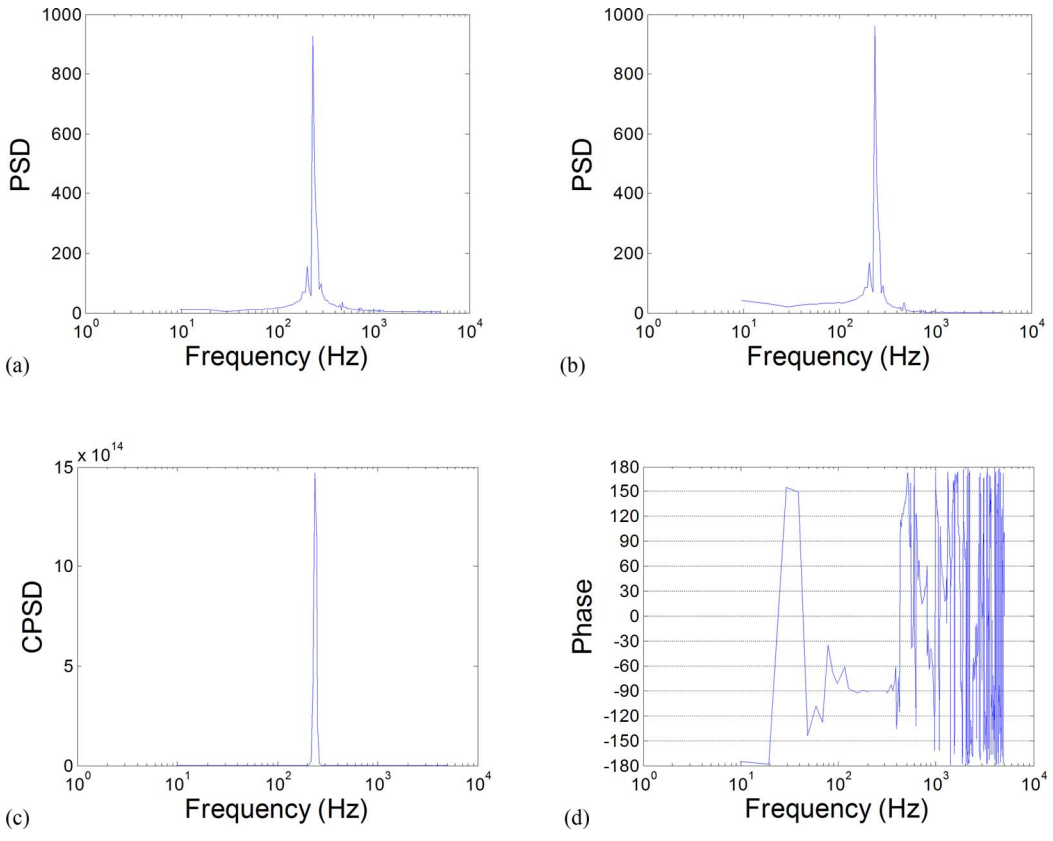

FIG. 8. Fourier transform of the temporal coefficient of POD modes 1 (a) and 2 (b) of the image ensemble of flow Re = 1635, We = 3.1, and MR = 10.1. A maximum at frequency 235 Hz can be observed for both cases. The cross spectral density of POD modes 1 and 2 (c) demonstrates the strong correlation between the two at frequency 235 Hz. The phase difference of the two modes is −90° at frequency 235 Hz, which is representative of wave propagation.

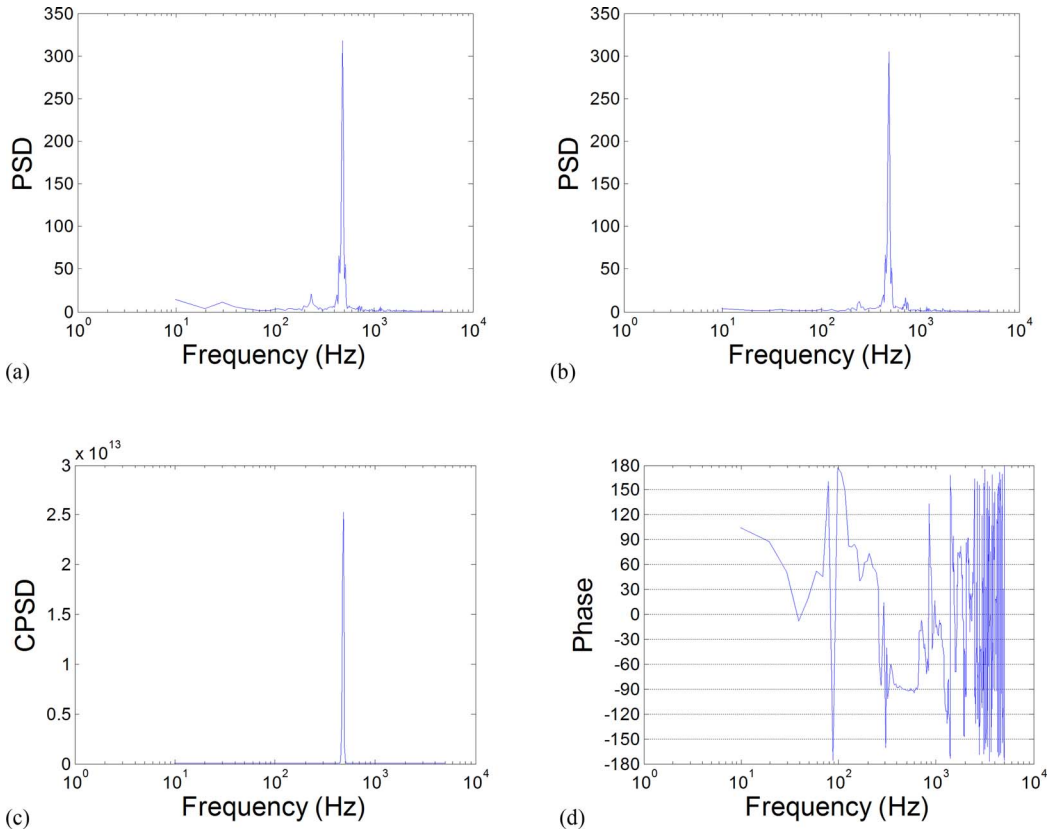

FIG. 9. Fourier transform of the temporal coefficient of POD modes 3 (a) and 4 (b) of the image ensemble of flow Re = 1635, We = 3.1, and MR = 10.1. A maximum at frequency 480 Hz can be observed for both cases. The cross spectral density of POD modes 3 and 4 (c) demonstrates the strong correlation between the two at frequency 480 Hz. The phase difference of the two modes is -90° at frequency 480 Hz, which is representative of wave propagation.

coefficients of POD modes 1 and 2 are shown, respectively. It can be seen that the two modes demonstrate identical temporal characteristics. The cross spectral density function, Figure 8(c), confirms this and shows a strong maximum at frequency 235 Hz. The phase relation between the two modes is shown in Figure 8(d) and it is clear that there is a phase difference of -90° between the two modes at frequency 235 Hz. The Fourier transform of the temporal coefficients of modes 3 and 4 also shows a definite periodicity with a frequency of 480 Hz for both modes (Figures 9(a) and 9(b)), which is about twice the frequency of the first harmonic. The correlation between the two is clear in Figure 9(c) and the phase swift of -90° between the two in Figure 9(d) confirms that their superposition represents the second harmonic of the varicose travelling wave. It is, therefore, unambiguously determined that the temporal frequency of the varicose dilatations is locked at 235 Hz for the considered flow with Re = 1635, We = 3.1, and MR = 10.1.

It should be noted that while this flow condition was selected for the description of the varicose regime, the POD description of the varicose flow with Re = 1907, We = 11.4, and MR = 7.4 is similar. The first four POD modes of this flow condition account for the majority of the image intensity fluctuations are morphologically identical to the POD modes described above, albeit with longer wavelengths, and the fundamental and harmonic frequencies are found at 235 Hz and at 480 Hz, respectively.

B. "Cup" shaped jet

The "cup" shaped jet development is an extension of the varicose mode when the initially round dilatation deforms and becomes progressively piriform and finally obtains an inverted cup shape.

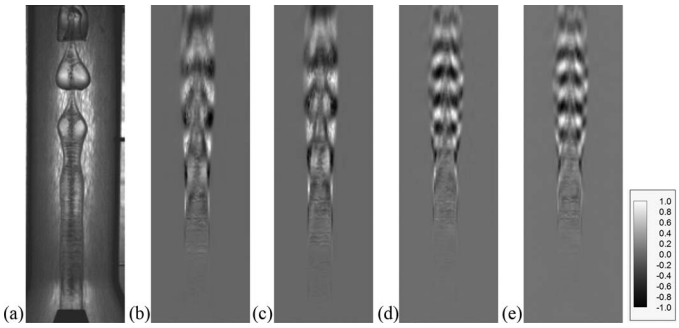

FIG. 10. Image sample of central liquid jet, (a), for flow Re = 2725, We = 67.7, MR = 3.6 and the first four POD modes, (b), (c), (d), and (e), respectively.

The POD analysis of the image samples breaks down the morphology of the development to modes, which are indicative of these geometries. As in the case of the varicose type of development, the overall shape of the developing jet can be described by two pairs of POD modes. An example is shown in Figure 10 for the flow with Re = 2725, We = 67.7, and MR = 3.6, which is the flow condition where the "cup" features are better developed. A sample image of the cup shaped jet is shown in Figure 10(a). The first two POD modes of this flow condition that capture the major morphology are presented in Figures 10(b) and 10(c). Close to the nozzle exit alternate white and black bands capture the initial varicose dilatation. However, further downstream the alternating bands obtain an oblique shape that captures the piriform shape of the cup structures. The two modes are complementary and express travelling waves. The second pair of complementary POD modes, shown in Figures 10(d) and 10(e), has half the spatial period of the first two modes in the longitudinal direction and captures the finer details of the development of the cup morphology. The reconstruction of the original jet image using these four modes is satisfactory and sufficient to describe the fundamental geometry of this type of flow. This can be confirmed by the quality of the image reconstruction that can be achieved using these modes. An example is shown in Figure 11, where the original image of Figure 11(a) is reconstructed using the first pair of POD modes, Figure 11(b), and in Figure 11(c) the two sets of POD modes are used for the reconstruction. The first pair is sufficient to capture the motion of the large scale structures. The reconstruction quality improves significantly with consideration of the second pair of POD modes. This occurs because this flow is more complex than the varicose flow and the jet characteristics are contained in more POD modes. This is confirmed in Figure 12, where it can be seen that the two first POD modes capture only about 25% of the intensity fluctuations of the jet images and the first four POD modes capture about 45% of the intensity fluctuations of the jet images.

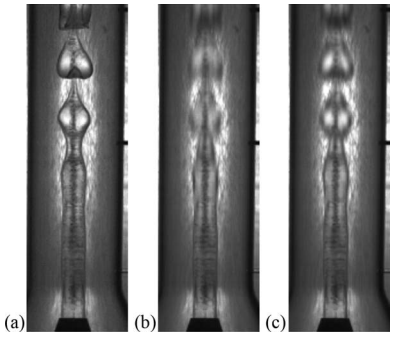

FIG. 11. Reconstruction of an image sample of liquid jet for flow Re = 2725, We = 67.7, MR = 3.6. (a) Original image, (b) reconstruction using modes 1 and 2, and (c) reconstruction using modes 1–4. Modes 1 and 2 capture the basic jet morphology and modes 3 and 4 capture the finer details.

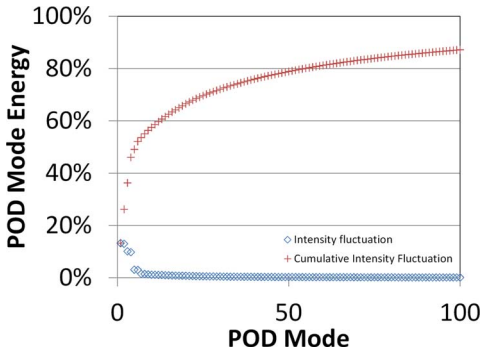

FIG. 12. Distribution of the normalised image intensity fluctuations that is captured by each POD mode and the cumulative normalised energy fluctuations for flow Re = 2725, We = 67.7, and MR = 3.6. The first four modes capture over 25% of the overall intensity fluctuations of the jet images.

The temporal analysis of the POD modes demonstrates that there exists a maximum at frequency 235 Hz for the first two modes, Figures 13(a) and 13(b). The cross spectral density of the two modes, Figure 13(c), confirms the temporal correlation of the two modes at frequency 235 Hz. The phase relationship between the two, Figure 13(d), shows a phase shift and supports that their combined effect is the creation of a travelling wave, which describes the development of the "cup" type instability. A minor maximum at the frequency of 480 Hz is also present in the PSD, which is due to

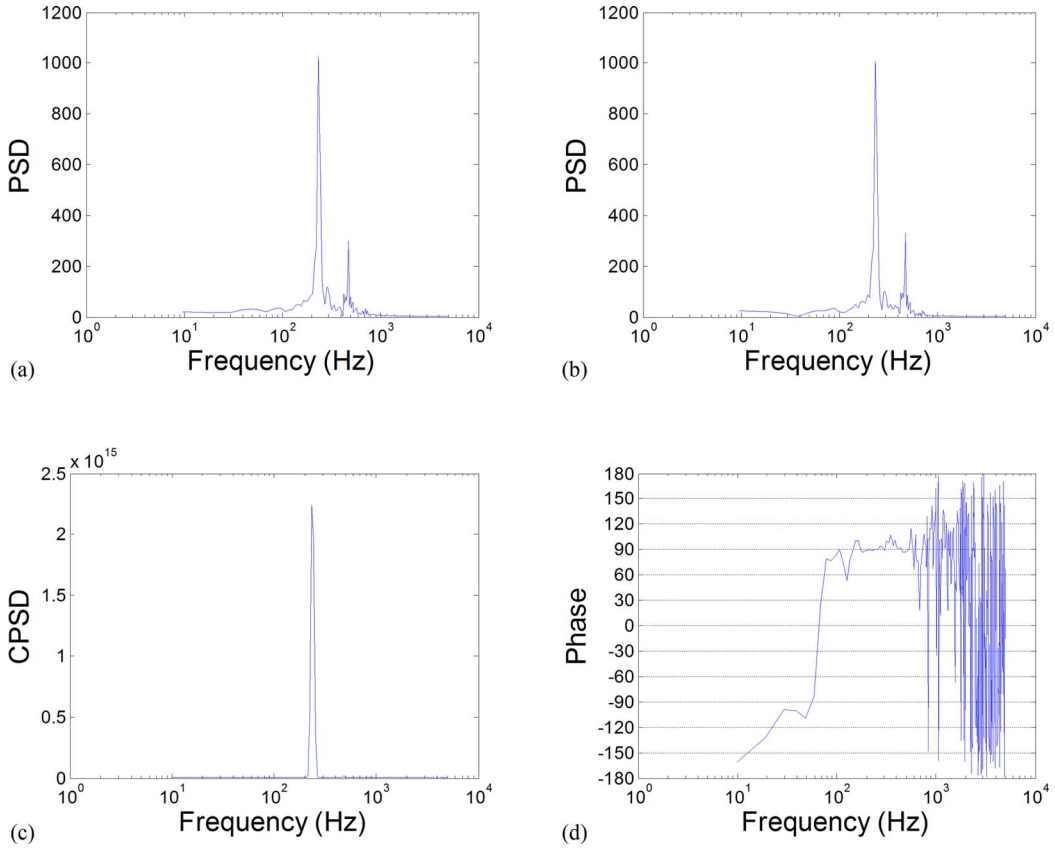

FIG. 13. Fourier transform of the temporal coefficient of POD modes 1 (a) and 2 (b) of the image ensemble of flow Re = 2725, We = 67.7, and MR = 3.6. A maximum at frequency 235 Hz can be observed for both cases. The cross spectral density of POD modes 1 and 2 (c) demonstrates the clear correlation between the two at frequency 235 Hz. The phase difference of the two modes is 90° at frequency 235 Hz, which is representative of wave propagation.

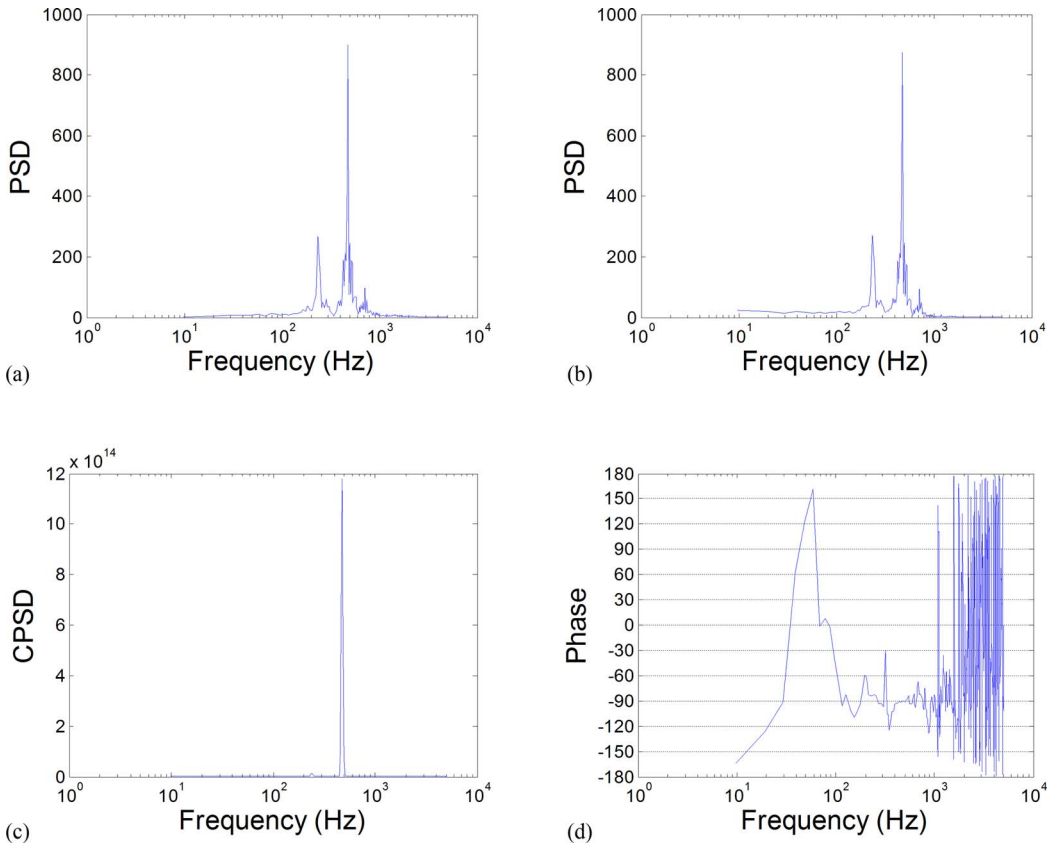

FIG. 14. Fourier transform of the temporal coefficient of POD modes 3 (a) and 4 (b) of the image ensemble of flow Re = 2725, We = 67.7, and MR = 3.6. A maximum at frequency 480 Hz can be observed for both cases. The cross spectral density of POD modes 3 and 4 (c) demonstrates the clear correlation between the two at frequency 480 Hz. The phase difference of the two modes is -90° at frequency 480 Hz, which is representative of wave propagation.

harmonic interference noise. This peak vanishes in the CPSD which suggests that the contribution of the 480 Hz component of the first two POD modes in the travelling wave is insignificant.

The temporal analysis of the second pair of POD modes is shown in Figure 14(d). The maxima of the two modes, Figures 14(a) and 14(b), are located at frequency 480 Hz with a phase shift of -90°, Figure 14(d). The correlation of these two modes is excellent as evident by the CPSD in Figure 14(c) and shows the second harmonic of the travelling wave described by the first two modes. A mirror peak in the PSD exists at the frequency 235 Hz for both of these POD modes. As explained above, there is some minor interference between the fundamental and the second harmonic. Nevertheless, the CPSD of the POD modes that describe the second harmonic shows that the interference between the fundamental and the second harmonic is insignificant.

The travelling waves described by the first POD modes for all the "cup" type and varicose type flows were found to be oscillating at the frequency 235 Hz for all of the considered flow conditions. This suggests that there is a fundamental excitation of the flow at this frequency.

C. Straight jet

Finally the straight type of jet flow is examined. This type of flow generally does not show many features. The main morphology that is captured is a rather slow flapping of the jet around its axis. This can be observed in the example of Figure 15 for the flow with Re = 545, We = −22.1, and MR = 91.4, which is the flow with the greatest acceleration of the central jet considered here. The flapping motion is periodic and this is captured in the geometrically complimentary POD modes 2

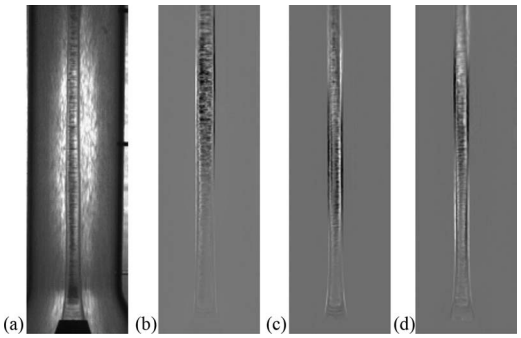

FIG. 15. Image sample of central jet (a) for flow Re = 545, We = −22.1 and MR = 91.8 and the POD mode 1 (b), 2 (c), and 3 (d).

and 3 shown in Figures 15(c) and 15(d), respectively. Together these two modes account for about 27% of the captured intensity fluctuation of the jet images, as shown in Figure 16. Although POD Mode 1, shown in Figure 15(b), accounts for 38% of the captured intensity fluctuation of the jet images, it does not contain information significant to the evolution of the jet morphology. It is more likely an indication of the overall range of oscillation of the jet rather than a description of a dynamic morphological feature.

The frequency analysis of the temporal coefficients of these modes, shown in Figures 17(a) and 17(b), demonstrates the periodicity of the flapping motion, which occurs at frequency 30 Hz. The cross spectral power of the temporal coefficients of these modes, Figure 17(c), and the phase shift of 90° between them, Figure 17, confirm that the motion is that of a travelling wave. Similar observations regarding the most energetic POD modes can be made for the straight jet flow with Re = 1090, We = −2.2, and MR = 22.8. However, for that flow condition, the oscillation of the straight jet occurs at frequency 20 Hz.

The above findings are in contrast to the findings for the varicose and "cup" type jets, where the most energetic POD modes were always found to occur at frequency 235 Hz and describe travelling waves. For this reason, the frequency spectra of the temporal coefficient of the less energetic higher order POD modes were examined looking for pairs of POD modes with the characteristic travelling wave morphology that occurs at frequency 235 Hz. While such a spatial mode would be undetectable by direct observation of the jet images, its presence was possible to be detected in POD modes 23 and 24, for the flow with Re = 545, We = −22.1, and MR = 91.4 and modes 5 and 6 for the flow with Re = 1090, We = −2.2, and MR = 22.8. For the flow with Re = 545, We = −22.1, and MR = 91.4, an example of which is shown in Figure 18, the contribution of this mode is very weak. The coherent spatial bands are faint and their intensity is comparable to the noise of the imaging system as it can be seen in Figures 18(b) and 18(c). This is because they only represent about 0.4% of the total energy captured by the POD analysis for this flow. Nevertheless, the frequency analysis

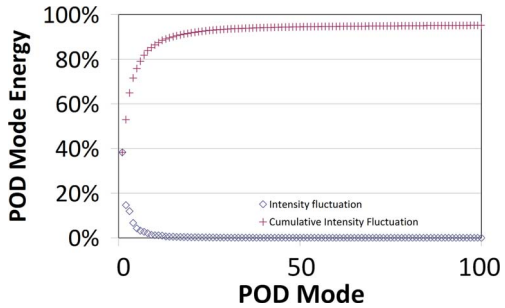

FIG. 16. Distribution of the normalised image intensity fluctuations that is captured by each POD mode and the cumulative normalised energy fluctuations for flow Re = 545, We = −22.1, and MR = 91.8.

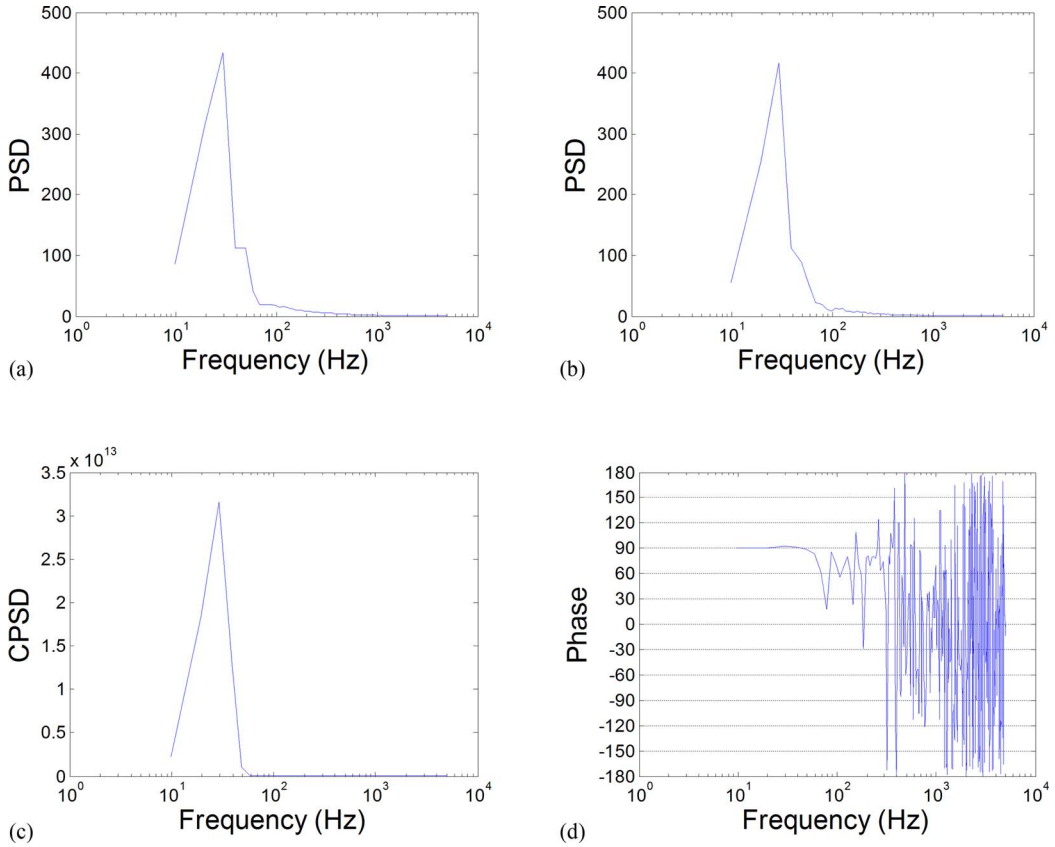

FIG. 17. Fourier transform of the temporal coefficient of POD modes 2 (a) and 3 (b) of the image ensemble of flow Re = 545, We = −22.1, and MR = 91.8. A maximum at frequency 30 Hz can be observed for both cases. The cross spectral density of POD modes 2 and 3 (c) demonstrates the strong correlation between the two at frequency 30 Hz. The phase difference of the two modes is 90° at frequency 30 Hz, which is representative of wave propagation.

of the temporal coefficients shows strong periodicity of these modes at the fundamental frequency of 235 Hz, Figures 19(a) and 19(b), along with the overtones. While the expression of the overtones is considerable, the increased noise in these POD modes must be taken into consideration. However, the CPSD shows that the correlation between the two modes is dominant at frequency 235 Hz, Figure 19(c), while the overtones are insignificant in the expression of the travelling wave. The phase between the two modes is around 90°, Figure 19(d).

For the straight flow with Re = 1090, We = −2.2, and MR = 22.8, the captured energy by the two POD modes that represent the interfacial wave at frequency 235 Hz, is about 5% and the

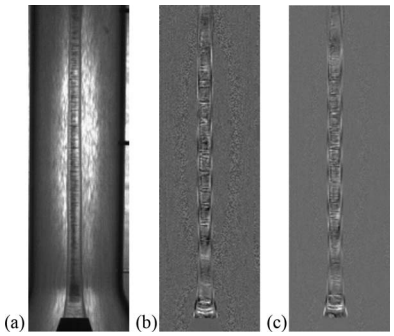

FIG. 18. Image sample of central liquid jet (a) for flow Re = 545, We = −22.1, and MR = 91.8 and the POD modes 23 (b) and 24 (c).

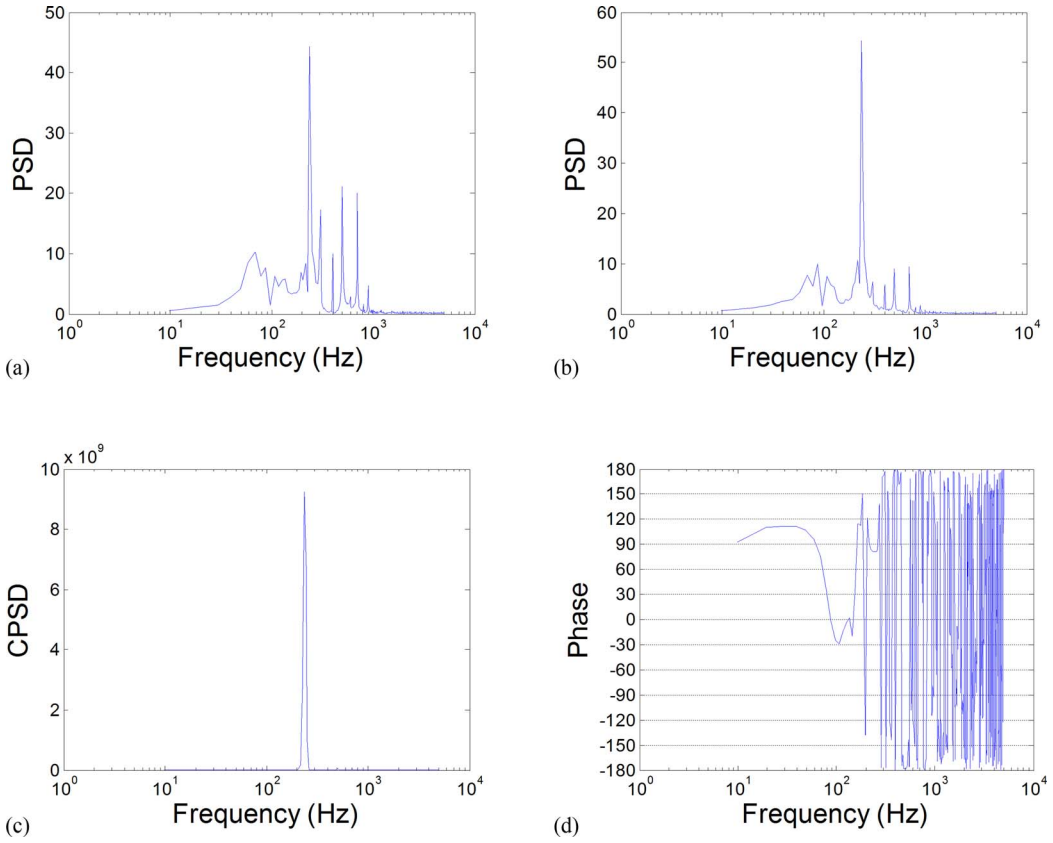

FIG. 19. Fourier transform of the temporal coefficient of POD modes 23 (a) and 24 (b) of the image ensemble of flow Re = 545, We = −22.1, and MR = 91.8. A maximum at frequency 235 Hz and its harmonics can be observed for both cases. The cross spectral density of POD modes 22 and 23 (c) demonstrates the strong correlation between the two at frequency 235 Hz. The phase difference of the two modes is about 90° at frequency 235 Hz.

phase relationship between the two modes is −90°, which is appropriate for a travelling wave. It can be concluded that the main observable movement of the jet is small oscillations of the jet around its axis, while there is always a travelling wave present at the frequency of 235 Hz with varying amplitude for different flows considered.

V. DISCUSSION

A description of the morphology of the central jet was provided in terms of the flow conditions. It was found that the central jet is straight when accelerated (negative We), it develops varicose dilatations for small central jet decelerations ($0 < We < 12$) and it develops a "cup" type of instability, which causes deformation of the jet, for higher deceleration of the central jet ($We > 12$). This demonstrates that the traditional characterisation of the destabilisation of two streams according to a We number based on the absolute velocity difference does not apply to confined coaxial jets. For the same $|We|$, we obtain very stable straight jets when there is acceleration (negative We) of the jet and unstable jets, which form "cup" structures and entrain the annular flow for decelerating jets (positive We). Therefore, the stability of the jet depends on the direction of the acceleration of the central jet. Conceptually, this can be understood by comparing the interface of a perturbed fluid cylinder that is being stretched to that of a perturbed fluid volume that is being compressed, as demonstrated in Figure 20. In the case of the former, a small perturbation will tend to decrease in amplitude as the cylinder stretches, Figure 20(a), while, for the latter, the amplitude of the perturbation will tend to increase as the cylinder compresses, Figure 20(b). In our flow, the shear between the two co-flowing streams will tend to initiate a Kelvin-Helmholtz type instability, which

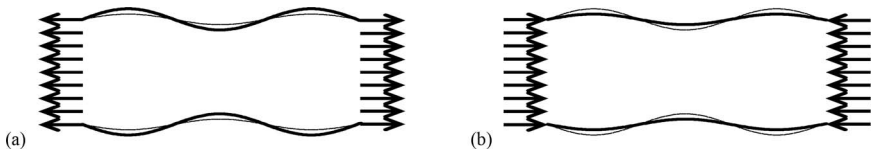

FIG. 20. Schematic of the effect of jet acceleration on its stability. (a) Stretching of the jet during acceleration causes instabilities to collapse and (b) compacting of the jet during deceleration causes instabilities to develop. Solid line indicates the original interface. Dashed line is the developed interface under the influence of jet acceleration.

will be undeveloped in the first case and amplified in the second to produce the observed flow patterns.

Further insight on the development of the flow was provided by the POD analysis of the jet images. It was determined that there is an omnipresent interfacial wave at a frequency 235 Hz. Its initial amplitude is small, since it cannot be detected by visual inspection of the straight jet images and it is only with POD that this interfacial wave can be detected in the straight flow regime as it accounts for only a small fraction of the total POD mode energy. For cases with instability development on the surface of the jet, this frequency dominates the production of the varicose dilatations and "cup" structures. The origin of this frequency is considered by evaluating previous experimental and theoretical research related to liquid injection and immiscible jet perturbation. Additionally, we consider alternative parameters that could affect the coaxial jet instability.

When reviewing the current knowledge on the development of immiscible coaxial jets, the most detailed investigations have been conducted on the instabilities on a liquid-gas interface for co-flowing streams.[7,28,29] The conclusion was that the dominant frequency depends mainly on the boundary layer thickness of the fast gas stream, the instability convection velocity and the density ratio. For our flows, where the outer stream velocity is constant, the boundary layer thickness should remain constant. For our density ratio and considering an annular boundary layer thickness of 1.0 mm and a convection velocity of the interface of 1 m/s, the dominant temporal frequency would be in the region of 1100 Hz. This value is over 4 times higher than the measured frequency in our experiments and depends on the velocities of the flow, which is not the case here. In order to obtain the same temporal frequency, the annular boundary layer thickness would need to be of the order of 5 mm, which is unlikely, considering that the annular flow is accelerated by a contraction before the nozzle tip. The investigations on the shearing liquid-gas interface are based on the premises of the annular flow velocity being much higher than the central jet velocity, the central to annular density ratio being large and the wave formation being dominated by the annular stream boundary layer thickness. These conditions deviate considerably from our case, since here the two streams can have similar velocities and densities and the growth rates of the shear layer thicknesses at each side of the interface are not expected to be completely dissimilar. Therefore, the conclusions of the investigations of the gas liquid shear investigations are not necessarily applicable here.

We have not been able to find experiments conducted on immiscible coaxial jets of similar densities. A number of studies of the development of the liquid jet in a liquid environment of an immiscible liquid have been conducted but have mainly focused on the breakup length of the jet and the wavelength of the instability.

The works of Tomokita[30] and Meister and Scheele[31] predict the interfacial wavelength as a function of the physical properties of the involved liquids only and does not take into account the relative velocities between the two streams. Even when the relative velocities between the two streams are close to the predicted wavelength from these theoretical studies is much larger than the observed. Kitamura *et al.*[32] considered the development of jets under zero relative velocity between the two streams and found that the hydrodynamic resistance of the continuous phase increases the growth rate of the disturbances but does not affect the instability wavelength. This is clearly not the case here where the wavelength was found to change even in the We ~ 0 limit for small changes of We. In a different investigation[33] the same researchers point out that the design of the nozzle can affect the development of the injected liquid in another liquid. In the investigation of Coyle *et al.*[34] on liquid jets injected in a quiescent liquid medium, it was found that with increasing Re, which in our

case is equivalent to a progressively increasing positive We (more decelerated jets), the wavelength of the instability decreases. Funada *et al.*[35] derived an explicit dispersion relation for temporal and convective/absolute instability. In their calculations the wavelength of the instability was also found to decrease with We. Overall, when looking into the current knowledge of jet development, we cannot find work related immediately to the type of the current flow.

We also consider sources of the dominant frequency, which are not due to the shear between the two coaxial streams but could excite it. The system pumps were considered. However their operating frequency is much lower than the identified frequency of 235 Hz. Additionally, the presence of filters between the pumps and the test section to capture micron size particles would have certainly removed any significant perturbation from any sources upstream. Another perturbation source that is considered is the operation of the flow chamber as a cavity. Considering that the annular phase is the dominant component of the flow, the frequencies for an open and closed resonator would be of the order of a few KHz for a cavity length of the size of the test section. A resonance frequency of around 235 Hz is found for a length of 1.5 m for an open cavity and 3 m for a closed cavity, which is far away for the length of the test section. The generation of vortex shedding within the flow circuit is also examined. Vortex shedding of a constant frequency would require a constant flow velocity. This in turn would imply that if such a perturbation would be related to the annular flow, which was kept constant while the central jet velocity was changed. The shedding frequency can be estimated as

$$f = \frac{St \cdot V}{T}, \tag{15}$$

where St is the Strouhal number, f is the vortex shedding frequency, T is the characteristic dimension, and V the characteristic velocity of the flow. The thickness of the wall of the central jet at the nozzle is a potential source of vortex shedding near the jet surface. For a Strouhal value of 0.21, a nozzle lip thickness of 1 mm, and a characteristic velocity of 0.96 m/s, the estimated frequency is 201 Hz. This is close to the observed dominant frequency of the oil jet. Therefore, it is possible that the injected jet is affected by vortex shedding at the nozzle lip. In this case, the intensity of the vortices is small since the oil jet does not seem to be significantly perturbed over some distance from the nozzle exit. It has been demonstrated before that the growth rate of the natural frequency of instabilities can be orders of magnitude greater when the system is excited[36] and that instabilities at other than those predicted from the hydrodynamic shear can become dominant, provided that there is sufficient excitation.[37] Therefore, for such a case, the importance of the design of the nozzle is highlighted.

While the temporal frequency of the features on the jet surface was found to be independent of the flow conditions, the wavelength, λ, of the interfacial waves, which can be measured with good accuracy from the well-defined boundaries of the POD modes, was found to depend on the Reynolds number. The dependence of the wavelength normalised to the exit diameter of the central jet on Re number is presented in Figure 21. The general trend is for the wavelength to increase with Re and the fitting of a linear trend between λ /D and Re seems to be appropriate. There is a clear difference

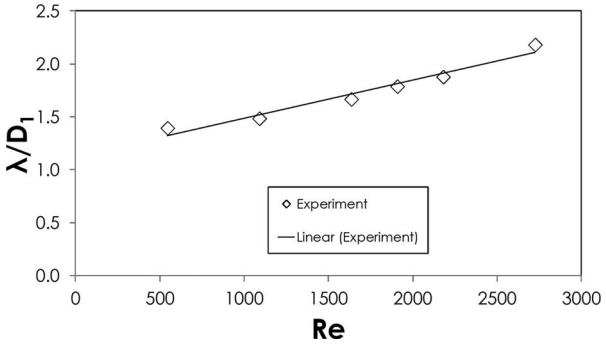

FIG. 21. Instability wavelength dependence on Re. The instability is associated with frequency 235 Hz detected for all flow conditions.

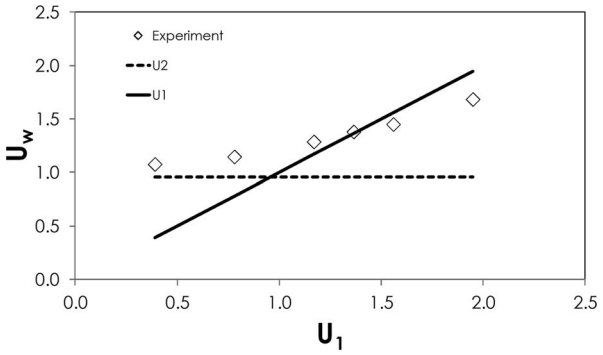

FIG. 22. Wave velocity of instability with frequency 235 Hz in relation to the bulk velocity of the central jet, U_1. The bulk velocity of the annular stream is $U_2 = 0.96$ m/s

between the current flow and the gas-liquid shearing flow investigations, since, in the latter, the wavelength decreases with Re for a fixed annular velocity.[7] This is also true for the thin vorticity layer limit where the wavelength decreases with the We number.

The dependence of the wavelength on Re is not perfectly linear and more insight is obtained when considering the velocity, U_w, of the waves at the interface. The wave velocity is obtained, from the instability wavelength and its corresponding frequency as

$$U_w = f\lambda. \tag{16}$$

The dependence of the wave velocity on flow conditions is presented in Figure 22 against the mean jet velocity. The mean jet velocity U_1 and the constant mean annular flow velocity $U_2 = 0.96$ m/s are also plotted for reference. When the central jet is accelerated, $U_1 < U_2$, the wave velocity is close to that of the annular stream, $U_w \sim U_2$. When the central jet is decelerated, $U_1 > U_2$, U_w becomes dependent on the velocity of the central jet stream, $U_w \sim U_1$. It is, therefore, apparent that the velocity of the wave on the jet interface depends on the velocity of the fastest of the two streams.

The most likely explanation of this dependence is that the interface is convected by the faster stream at the velocity of that stream. The reason can be sought at the momentum ratio between the two streams. In the case of accelerated central jets, the momentum of the annular flow is considerably greater, 20–90 times, than the momentum of the central jet flow. As a result the central jet is quickly accelerated close to the nozzle exit by the fast moving stream to the velocity of the annular stream and the instabilities at the interface are convected at that velocity. When the central jet velocity overcomes the annular jet velocity, its momentum, while still lower than that of the central jet, increases drastically so that $3.6 < \mathrm{MR} < 10.1$. As a result the central stream is now much less susceptible to the deceleration of the annular flow. It is then arguable that due to the low deceleration of the central jet, the interface is moving at a velocity that is close to that of the central jet. Velocity measurements across the interface could clarify the mechanism responsible. Such measurements had been attempted by means of Particle Image Velocimetry (PIV). However, due to issues related to particle seeding density close to the interface, particle seeding accumulation on the interface between the two liquids and laser sheet reflections from the interface of the two streams, the velocities could not be resolved. This is currently the focus of a future investigation, which will concentrate of the flowfield that is responsible for the development of the interfacial waves.

More useful information on the flow development is offered by the POD analysis when examining the spatial magnitude of the nodes. As the POD nodes represent the spatial extent of the interfacial instabilities, the area of the nodes expresses the size of the instabilities not only by considering the wavelength but also by considering the instability as a coherent structure. This is important because as the instability grows downstream of the jet, the amplitude of the instability increases considerably within a distance of one wavelength and the wave is not sinusoidal but develops in a piriform shape. An example for the need for this is information is shown in Figure 23(a), for the flow with Re = 2725, We = 67.7, and MR = 3.6. The second and third nodes along the liquid interface for the

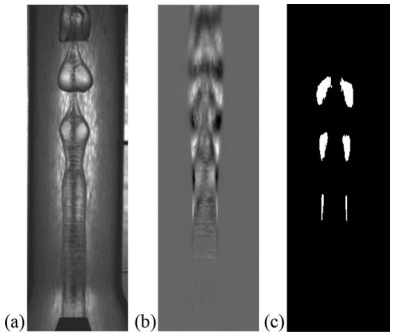

FIG. 23. Determination of area within the nodes of the POD modes. Example for flow with Re = 2725, We = 67.7, and MR = 3.6. (a) Example flow image, (b) POD mode 1, and (c) detected node area. The detected area increases considerably every wavelength downstream.

first POD mode, presented in Figure 23(b), demonstrate clearly that the non-sinus instability can be identified by POD, while Figure 23(c) demonstrates that the area that corresponds to the instability of each successive POD node downstream of the nozzle can be isolated for processing for a number of POD nodes until the jet becomes excessively deformed.

The area of the POD nodes associated with the traveling wave instability is presented in Figure 24 for the first three successive POD nodes in the order they appear from the nozzle exit, for all the considered flow conditions with the exemption of the flow with Re = 545, We = −22.1, and MR = 91.8. In that case, the wave is found in modes 23 and 24 and the area of the POD nodes could not be identified. For most flows, it can be seen that the area of the nodes, and consequently the magnitude of the instability, increases linearly between successive POD nodes, therefore with each successive interfacial wave. Consequently, the information provided by POD can serve as a tool to identify if the interface is developing in linear regime. The deviation from linearity is captured well for the most intensely decelerated flow (Re = 2725, We = 67.7, and MR = 3.6), where a reduction of the growth rate is observed within three interfacial waves.

By linear regression of the data in Figure 24, the slope of the area of the POD nodes is obtained along the first three POD nodes. The slope is equivalent to the rate of growth of the interfacial wave and can highlight the influence of the flow parameters. The wave growth rate is presented in Figure 25 as a function of the We number. It can be clearly seen that, as the We number increases, the growth rate of the wave increases proportionally for the flows where the instability develops linearly along successive POD nodes. The linear increase of the wave growth rate with We is retarded for the flow with Re = 2725, We = 67.7, and MR = 3.6, where the spatial growth is also limited with each successive POD node. The effect is less significant, if the growth rate is estimated for

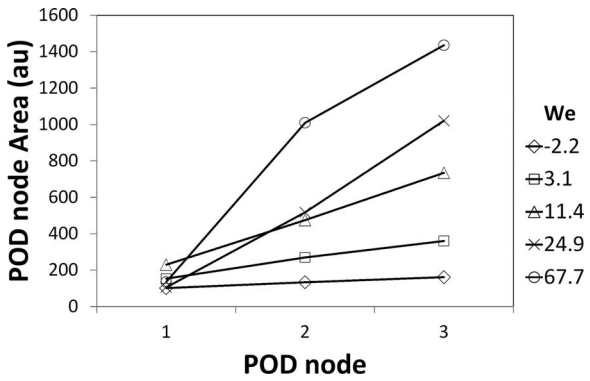

FIG. 24. Area of the POD nodes from the POD modes corresponding to 235 Hz, as a function of integral interfacial waves. For each successive node the area increases linearly while the slope is linear for all flows except for the flow with the highest jet We.

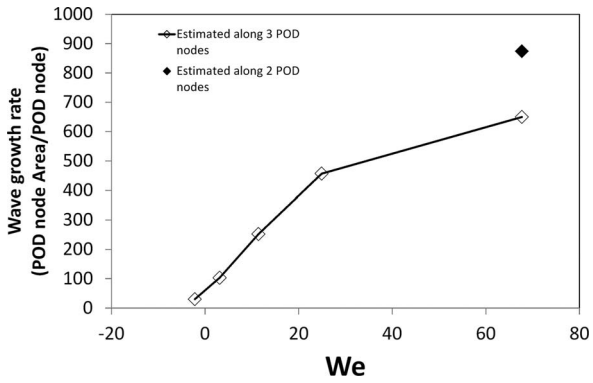

FIG. 25. Growth rate of the interfacial wave as determined by the rate of growth of the POD node area. As the We number increases, the rate of growth of the interfacial wave is linearly accelerated for all flows except for the flow with the highest We.

the two first POD nodes, which shows that the rate of the wave growth close to the nozzle exit is not affected considerably by nonlinear effects. Considering the linear growth of the interfacial waves, stability analysis would be an appropriate tool for the evaluation of the findings of the current study, which would highlight the mechanisms responsible for this type of jet development. The above findings demonstrate the mostly linear development of the interfacial waves in the near nozzle region for liquids of similar densities and viscosities. However, these findings may not apply to liquids with dissimilar densities and viscosities. Therefore, further investigation on the growth of the interfacial waves is warranted over a range of relative physical properties to resolve their influence on development of the two streams, which would determine the appropriate type of theoretical approach required for the analytical examination of such instabilities.

VI. CONCLUSIONS

The morphology of the development of a circular oil jet under the influence of a coaxial stream of water was investigated within the bounds of a tubular channel in the vicinity of accelerated and decelerated central jets. The flow was described in terms of the Reynolds number, the Weber number and the annular to central jet momentum ratio. Re was in the range between 545 and 2725, We was in the range between −22.1 and 67.7, and MR was in the range between 3.6 and 91.4. The central to annular flow density ratio was 8:10. Three modes of the central oil jet development were observed, namely the straight jet flow, the varicose jet flow and the "cup" type flow. The first mode is produced when the jet is accelerated and the other two modes develop when the jet is decelerated by the annular flow. The conventional approach of defining the We number with the absolute velocity difference was inadequate for the description of the observed flow patterns, as no distinction is provided between accelerated and decelerated jets. It is proposed that a sign is required for the We number (see definition of Eq. (10)), to distinguish between accelerated central jets (negative We) and decelerated central jets (positive We).

The morphology of the developing central jet was analysed using Proper Orthogonal Decomposition of the temporally resolved image sequences, reducing the description of the developing jet to a small number of spatially coherent structures. In this way, the basic morphological structures of the interface can be resolved and interfacial features can be detected, which would be unobtainable using conventional image analysis. Through POD analysis, a travelling wave at frequency 235 Hz was found to exist. The amplitude of the wave at this frequency was minimal in flows where the central jet is accelerated and could only be observed using POD. When the central jet is decelerated, the traveling wave grew to dominate the formation of interfacial instabilities in flows.

The elongation of the central jet during acceleration is unfavourable to instability growth, while the compaction of the central jet during deceleration favours instability growth. The velocity of the waves at the interface was found to closely match the velocity of the fastest moving flow. This is

attributed to the annular to central stream momentum ratio because, for accelerating jets, MR is large and the annular stream dominates the central jet while for decelerated jets MR decreases and the central jet is less susceptible to the annular flow. The wavelength of the developing instabilities was found to depend on the velocity of the fastest moving stream.

In addition to the identification of morphological features of the interface using POD, it was possible to extract the spatial growth of the interfacial waves by considering the magnitude of the POD nodes. Through POD analysis, it was possible to capture the non-sinusoidal development of the jet. The interfacial waves are found to grow linearly with the distance from the nozzle for We ≤ 25. The rate of growth of the interfacial waves was found to depend strongly on We and remain linear until We ~ 25 and continue to increase at a reduced rate thereafter.

ACKNOWLEDGMENTS

The authors acknowledge financial support from the Engineering and Physical Sciences Research Council (EPSRC) through grants EP/F009194/1 and EP/G01597X/1.

[1] S. P. Lin and R. D. Reitz, "Drop and spray formation from a liquid jet," Annu. Rev. Fluid Mech. **30**, 85–105 (1998).
[2] J. C. Lasheras and E. J. Hopfinger, "Liquid jet instability and atomization in a coaxial gas stream," Annu. Rev. Fluid Mech. **32**, 275–308 (2000).
[3] A. H. Lefebvre, *Atomization and Sprays* (Hemisphere Publishing Corporation, 1989).
[4] H. Eroglu, N. Chigier, and Z. Farago, "Coaxial atomizer liquid intact lengths," Phys. Fluids A **3**(2), 303–308 (1991).
[5] C. Engelbert, Y. Hardalupas, and J. H. Whitelaw, "Breakup phenomena in coaxial airblast atomizers," Proc. R. Soc. London, Ser. A **451**(1941), 189–229 (1995).
[6] J. C. Lasheras, E. Villermaux, and E. J. Hopfinger, "Break-up and atomization of a round water jet by a high-speed annular air jet," J. Fluid Mech. **357**, 351–379 (1998).
[7] P. H. Marmottant and E. Villermaux, "On spray formation," J. Fluid Mech. **498**, 73–111 (2004).
[8] C. M. Varga, J. C. Lasheras, and E. J. Hopfinger, "Initial breakup of a small-diameter liquid jet by a high-speed gas stream," J. Fluid Mech. **497**, 405–434 (2003).
[9] R. Domann and Y. Hardalupas, "Breakup model for accelerating liquid jets," 42nd AIAA Aerospace Sciences Meeting and Exhibit, Reno, Nevada, 2004.
[10] G. Charalampous, Y. Hardalupas, and A. M. K. P. Taylor, "Destabilization modes of confined coaxial liquid jets," 6th International Conference on Multiphase Flow, Tampa, USA, 2010.
[11] D. R. Webster and E. K. Longmire, "Jet pinch-off and drop formation in immiscible liquid-liquid systems," Exp. Fluids **30**(1), 47–56 (2001).
[12] I. N. Milosevic and E. K. Longmire, "Pinch-off modes and satellite formation in liquid/liquid jet systems," Int. J. Multiphase Flow **28**(11), 1853–1869 (2002).
[13] S. Homma, J. Koga, S. Matsumoto, M. Song, and G. Tryggvason, "Breakup mode of an axisymmetric liquid jet injected into another immiscible liquid," Chem. Eng. Sci. **61**(12), 3986–3996 (2006).
[14] B. J. Meister and G. F. Scheele, "Prediction of jet length in immiscible liquid systems," AIChE J. **15**(5), 689–699 (1969).
[15] B. J. Meister and G. F. Scheele, "Drop formation from cylindrical jets in immiscible liquid systems," AIChE J. **15**(5), 700–706 (1969).
[16] L. Tadrist, E. K. O. Alaoui, R. Occelli, and J. Pantaloni, "Experimental study of a liquid jet flowing into another immiscible liquid "a local analysis of the interface"," Exp. Fluids **12**(1), 67–75 (1991).
[17] O. A. Basaran, "Small-scale free surface flows with breakup: Drop formation and emerging applications," AIChE J. **48**(9), 1842–1848 (2002).
[18] H. A. Stone, A. D. Stroock, and A. Ajdari, "Engineering flows in small devices: Microfluidics toward a lab-on-a-chip," Annu. Rev. Fluid Mech. **36**, 381–411 (2004).
[19] A. Barrero and I. G. Loscertales, "Micro- and nanoparticles via capillary flows," Annu. Rev. Fluid Mech. **39**, 89–106 (2007).
[20] K. Pearson, "On lines and planes of closest fit to systems of points in space," Philos. Mag. **2**(6), 559–572 (1901).
[21] J. Lumley, in *Atmospheric Turbulence and Wave Propagation*, edited by A. Yaglom and V. Tatarski (Nauka, Moscow, 1967), pp. 166–178.
[22] G. Berkooz, P. Holmes, and J. L. Lumley, "The proper orthogonal decomposition in the analysis of turbulent flows," Annu. Rev. Fluid Mech. **25**, 539–575 (1993).
[23] L. Sirovich and M. Kirby, "Low-dimensional procedure for the characterization of human faces," J. Opt. Soc. Am. A **4**(3), 519–524 (1987).
[24] M. Arienti and M. C. Soteriou, "Time-resolved proper orthogonal decomposition of liquid jet dynamics," Phys. Fluids **21**(11), 112104 (2009).
[25] G. I. Barenblatt, *Scaling* (Cambridge University Press, 2003).
[26] C. Z. Weber, "Zum zerfall eines flussigkeitsstrahles," Math. Mech. **11**(2), 136–159 (1931).
[27] L. Bayvel and Z. Orzechowski, *Liquid Atomization* (Taylor & Francis, 1993).
[28] J. P. Matas, S. Marty, and A. Cartellier, "Experimental and analytical study of the shear instability of a gas-liquid mixing layer," Phys. Fluids **23**(9), 094112 (2011).

[29] E. Villermaux, "Mixing and spray formation in coaxial jets," J. Propul. Power **14**(5), 807–817 (1998).
[30] S. Tomotika, "On the instability of a cylindrical thread of a viscous liquid surrounded by another viscous fluid," Proc. R. Soc. London, Ser. A **150**(870), 322–337 (1935).
[31] B. J. Meister and G. F. Scheele, "Generalized solution of the tomotika stability analysis for a cylindrical jet," AIChE J. **13**(4), 682–688 (1967).
[32] Y. Kitamura, H. Mishima, and T. Takahashi, "Stability of jets in liquid-liquid systems," Can. J. Chem. Eng. **60**(6), 723–731 (1982).
[33] T. Takahashi and Y. Kitamura, "Effect of nozzle length on breakup length of liquid jet," Mem. Sch. Eng., Okayama Univ. **4**(1), 57–64 (1969).
[34] R. W. Coyle, J. C. Berg, and J. C. Niwa, "Liquid-liquid jet breakup under conditions of relative motion, mass transfer and solute adsorption," Chem. Eng. Sci. **36**(1), 19–28 (1981).
[35] T. Funada, D. D. Joseph, and S. Yamashita, "Stability of a liquid jet into incompressible gases and liquids," Int. J. Multiphase Flow **30**(11), 1279–1310 (2004).
[36] J. M. Kendall, "Experiments on Annular liquid jet instability and on the formation of liquid shells," Phys. Fluids **29**(7), 2086–2094 (1986).
[37] G. E. A. Meier, A. Klopper, and G. Grabitz, "The influence of kinematic waves on jet break down," Exp. Fluids **12**(3), 173–180 (1992).